

Ferromagnetic fragmented ground state in the pyrochlore $\text{Ho}_2\text{Ru}_2\text{O}_7$

F. Museur,^{1,2,*} J. Robert,¹ F. Morineau,¹ V. Simonet,¹ E. Pachoud,¹ A. Hadj-Azzem,¹
C. Colin,¹ P. Manuel,³ J. R. Stewart,³ P. C. W. Holdsworth,² and E. Lhotel¹

¹*Institut Néel, CNRS & Univ. Grenoble Alpes, 38042 Grenoble, France*

²*ENS de Lyon, CNRS, Laboratoire de Physique, F-69342 Lyon, France*

³*ISIS Facility, Rutherford Appleton Laboratory-STFC, Chilton, Didcot, OX11 0QX, United Kingdom*

The consecutive magnetic ordering of the Ho and Ru ions in the pyrochlore $\text{Ho}_2\text{Ru}_2\text{O}_7$ and their interplay are investigated by neutron scattering, magnetic and specific heat measurements. The Ru magnetic moments order at 95 K into an easy-plane antiferromagnetic state, while the Ho moments order at 1.55 K into an unsaturated ferromagnetic state that retains an extensive ground state entropy and present complex spin dynamics throughout the low temperature phase. These unexpected features are analyzed in terms of a fragmented ferromagnetic state equivalent to the pyrochlore kagome ice. Selection of this unusual state relies on a subtle compromise between long-range ferromagnetic interactions between holmium moments and a repulsive cubic field, both mediated by the ruthenium lattice.

Highly frustrated magnets [1] have proved a rich source of materials showing novel, strongly correlated phases of matter. Among the most striking examples are holmium and dysprosium titanates, the original spin ice materials [2, 3] in which the magnetic Ho^{3+} and Dy^{3+} ions lie on a pyrochlore lattice, occupying the A sites of the $A_2B_2O_7$ structure (Fig. 1a). The B sites, occupied by the non-magnetic Ti^{4+} ions form a second, interpenetrating pyrochlore lattice. Spin ices are frustrated ferromagnets in which strong crystal fields and combined exchange and dipole interactions result in effective first neighbour ferromagnetic exchange [4]. The materials remain disordered down to 50 mK, way below the magnetic interaction scale, with the spins satisfying the ice rules of two spins pointing into and two pointing out of each tetrahedron [5, 6]. Great strides have been made in the understanding of these complex systems through the identification of an emergent gauge field description [7, 8] with associated topological defects, magnetic monopoles [9, 10]. This fractionalisation of magnetic moments into deconfined magnetic monopoles and the emergence of continuous symmetry from discrete, Ising like degrees of freedom, is captured in full by the process of fragmentation [11, 12]. In this field theoretic formalism, the magnetic moments appear to separate, via a Helmholtz decomposition into a particle sector and left over gauge and harmonic sectors [13, 14].

Replacing the titanium by magnetic ions such as iridium or ruthenium adds to the richness of the emergent description. The ions on the B sites now order on the 100 K temperature scale [18, 19], providing strong internal fields that act on the A sites at the energy scale associated with magnetic monopole physics. In the case of iridates, “all in - all out” (AIAO) iridium ordering creates a strong staggered molecular field along the Dy^{3+} or

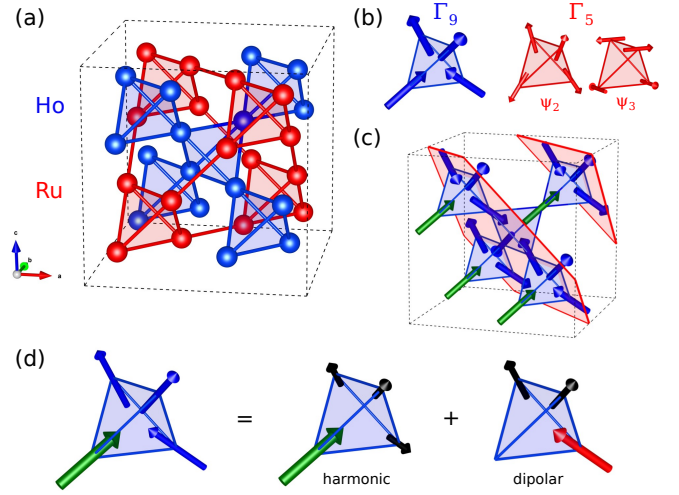


FIG. 1. (a) The $\text{Ho}_2\text{Ru}_2\text{O}_7$ pyrochlore lattice; Ho sublattice in blue and Ru sublattice in red. (b) Ordered spin structure from the Γ_9 representation (left) and two states ψ_2 and ψ_3 from which easy-plane antiferromagnetic structures belonging to the Γ_5 representation can be built (right) (See for example Refs. 15–17 for the definition of these representations). (c) Ferromagnetic fragmented magnetic structure. (d) Graphical representation of the magnetic fragmentation (Equation 1) for the proposed scenario in $\text{Ho}_2\text{Ru}_2\text{O}_7$. The green spin is the apical spin and the red spin is the majority moment of the dipolar fragment.

Ho^{3+} moments which stabilises an ordered 3 out - 1 in / 3 in - 1 out state, although there is no further phase transition [20–22]. Within the fragmentation picture the particle sector yields a monopole crystal with the zinc-blend structure and the gauge sector is that of emergent hard-core dimers on the diamond lattice of tetrahedra centres [11, 12, 23, 24]. The partial ordering manifests itself in neutron experiments by the coexistence of AIAO order and diffuse scattering characteristic of a Coulomb phase, with 50 % of the scattering amplitude in each sector [11, 20]. Specific heat experiments recover the resid-

* Contact: flavien.museur@psi.ch; Current address: Laboratory for Mesoscopic Systems, Paul Scherrer Institut and ETH Zurich, 8093 Zurich, Switzerland.

ual entropy of the dimer system [21].

In ruthenates there is a further transition at low temperature (1.85 K and 1.55 K for Dy and Ho respectively) [19, 25] but to an unsaturated phase again with a residual entropy [26, 27]. Neutron diffraction experiments on a powder sample of $\text{Ho}_2\text{Ru}_2\text{O}_7$ were consistent with a ferromagnetic, Γ_9 spin ice state (See Fig. 1b) with an ordered moment of about $6.3 \mu_B$ per spin, considerably reduced from the full $10 \mu_B$ per holmium ion [28]. These two puzzling features have not been understood to date. In this paper, through neutron scattering, specific heat and magnetisation studies on a powder sample of $\text{Ho}_2\text{Ru}_2\text{O}_7$, we show that this ordering is consistent with a novel, fragmented ground state with magnetisation aligned along one of the body centred cubic [111] axes as illustrated in Fig. 1c. In addition, we observe in the ac susceptibility unusual dynamics, with a discontinuity in the characteristic relaxation times associated with the holmium transition.

The sample was synthesized by solid state reaction from the oxide precursors Ho_2O_3 and RuO_2 , with a small excess (5% mol) of RuO_2 following Ref. 29. The powders were finely ground, pressed in a pellet and reacted at 1000°C in air for 48 h, then 1100°C in a platinum tube inside an evacuated sealed silica tube for 12 days with intermediate grindings. An X-ray diffraction analysis of the crystal structure post synthesis revealed the presence of 1.58 % of Ho_2O_3 , visible as small peaks in neutron diffractogram (see Fig. 2b). Magnetometry measurements were performed on a MPMS VSM squid magnetometer between 2 and 300 K and SQUID magnetometers equipped with a dilution refrigerator developed at the Institut Néel between 70 mK and 4.2 K [30]. Specific heat measurements were performed on a PPMS apparatus between 350 mK and 300 K. Neutron diffraction measurements were performed on D1B - CRG@ILL [31] and WISH@ISIS [32, 33]. Inelastic neutron scattering measurements were performed on LET@ISIS [34, 35] (See Supplementary Material [36]).

Specific heat measurements show a transition at 95 K [36] consistently with previous studies [19, 25]. In Fig. 2a we show neutron scattering data at 31 K which highlights the Ru ordering. The magnetic structure was previously interpreted as ferromagnetic, belonging to the Γ_9 spin ice state [28]. However, such an ordering would be characterised by a Bragg peak at the (002) position [17], indicated by the blue arrow. Our data which profits from better statistics does not resolve this peak and in its absence peaks at the (111) and (220) positions are consistent with an easy-plane $Q = 0$ state belonging to the Γ_5 representation (See Fig. 1b), as reported in other pyrochlore ruthenates [19, 38]. Note that the exact spin configuration within the Γ_5 manifold cannot be obtained from powder neutron diffraction [16]. The intensity of the magnetic peaks saturates below 75 K and a Rietveld refinement gives an ordered ruthenium moment of around $1.2 \mu_B$.

The holmium magnetic structure at low temperature

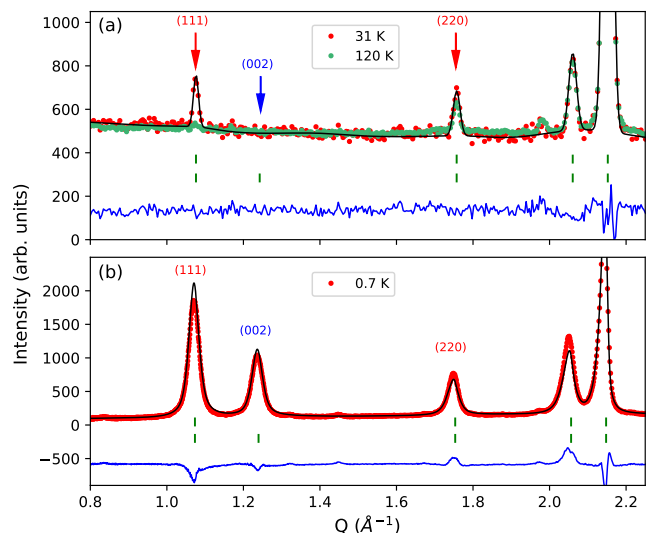


FIG. 2. Neutron diffractograms: (a) at 31 and 120 K showing the Ru magnetic ordering, measured on D1B@ILL; (b) at 0.7 K showing the Ho magnetic ordering, measured on WISH@ISIS. Dark lines are the Rietveld refinements performed with the FULLPROF software [37], with the Γ_5 and Γ_9 representations (See Fig. 1) for Ru and Ho respectively [36]. Blue lines are the differences between the fit and the data and green ticks index the Bragg peaks. The (002) peak, present in the Γ_9 representation but absent in Γ_5 , only appears below the Ho transition.

(See Fig. 2b), is consistent with ferromagnetic spin ice belonging to the Γ_9 representation, with a refined ordered moment of around $6.5 \mu_B$ per Ho at 300 mK [36], similarly to Ref 28. Down to the base temperature, the magnetic Bragg peaks remain broader and more symmetric than the nuclear peaks showing the characteristic time-of-flight lineshape. This indicates that the order is made up of mesoscopic domains, which were estimated from the full width at half maximum of the (002) peak to be of the order of 100 \AA , corresponding to roughly ten elementary cubic units or 1600 spins.

The sample enters the Ho ordered phase via a transition, with a very sharp peak in the magnetic specific heat $T_c \approx 1.55 \text{ K}$ (See Fig. 3a). The singularity resists fields up to 0.1 T but is smoothed out for higher fields. This temperature is the typical interaction scale for spin ice physics in $\text{Ho}_2\text{Ti}_2\text{O}_7$ [3]. The transition manifests itself as a sharp increase in magnetization, as shown in Fig. 3c. A large Zero Field Cooled - Field Cooled (ZFC-FC) irreversibility develops below the transition, indicating the presence of significant energy barriers. ac susceptibility measurements as a function of temperature show the presence of frequency dependent dynamic behaviour, which persists below the transition.

At fixed temperature, the imaginary part of the ac susceptibility, $\chi''(\omega)$ (See Fig. 4), is characterized by two peaks, present over the whole temperature range, corresponding to a rapid and a slow process. This signal is

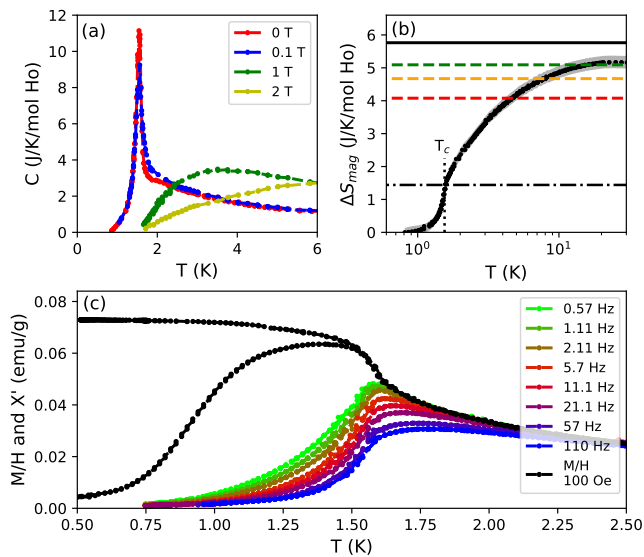


FIG. 3. (a) Magnetic specific heat in zero field and for applied fields, corrected for nuclear hyperfine and phonon contributions [36]. (b) Magnetic entropy difference with the expected values for spin ice (red), a monopole crystal (orange), kagome ice (green), $R \ln(2)$ (full black), $\frac{1}{4} R \ln(2)$ (dashed black). (c) In-phase part of the ac susceptibility as a function of temperature, together with the magnetization to field ratio measured in a ZFC-FC protocol with a field of 100 Oe (black).

reminiscent of that for $\text{Ho}_2\text{Ti}_2\text{O}_7$ [39, 40], and the persistence of well defined dynamic behaviour below the ordering temperature calls to mind experiments on $\text{Ho}_2\text{Ir}_2\text{O}_7$ [20]. The two time scales can be extracted from our susceptibility data from a generalized Debye analysis [36] (see Fig. 4b). The relative amplitudes of the two processes vary with temperature. Above the transition, the dominant fast process approaches an Arrhenius law with an energy of about 6 K, close to the value of the monopole chemical potential in $\text{Ho}_2\text{Ti}_2\text{O}_7$, $-\mu = 5.8$ K [10, 41]. This suggests relaxation via the dynamics of deconfined monopoles. At the transition the amplitudes are equal and the transition signifies a change in the dominant relaxation process. Below the transition the prevailing slow process evolves towards a characteristic energy scale of 15 K. These persistent and sizeable dynamics at low temperature point to an unconventional ordered state with well-defined excitations.

Indeed, a residual entropy is observed (See Fig. 3b), as previously reported [27]. This does not match the Pauling estimate for spin ice though [5], nor does it correspond to that for a fragmented monopole crystal [11]. However, it does correspond to a documented value from the spin ice literature, that for the magnetisation plateau for spin ice in the presence of a field of moderate strength applied along the [111] crystal axis [42, 43], the so-called kagome ice state. The residual entropy is therefore consistent with a novel state, a ferromagnetic phase with broken symmetry along one of the [111] axes, the *ferromag-*

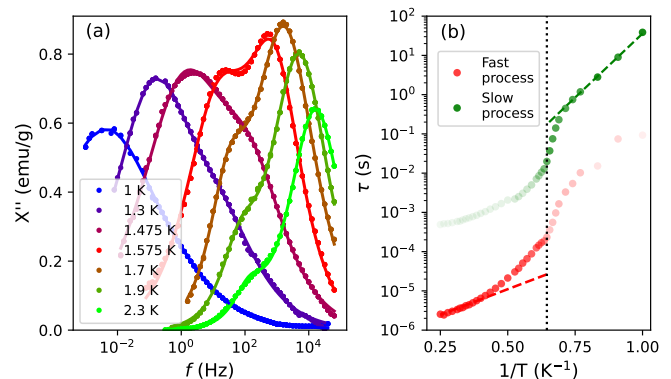


FIG. 4. (a) ac susceptibility as a function of frequency at fixed temperatures. (b) relaxation times from a fit to a generalized Debye function with two characteristic relaxation times [36]. The transparency of the symbols indicate the relative amplitude of the two processes. Dotted lines, Arrhenius laws $\tau = \tau_0 \exp(E/T)$, with $\tau_{0f} = 5.5 \times 10^{-7}$ s and $E_f = 6$ K above T_c and $\tau_{0s} = 1.1 \times 10^{-5}$ s and $E_s = 15$ K below.

netic fragmented state which features decoupled kagome planes of magnetic moments lying perpendicular to the field axis. Such a phase requires a distinction between the four spins of a tetrahedral unit cell, as highlighted in Fig. 1c. The apical spin (shown in green) would be frozen and aligned along the broken symmetry axis with an entropy drop of approximately $(\frac{R}{4}) \ln 2$, as observed in our data at the transition. The three spins lying in the kagome plane (in red) would then satisfy the kagome ice rules of two spins in - one spin out [44, 45].

This is another example of a fragmented ground state in which identifiable ordered and disordered fragments coexist. In this case, the ground state is a monopole vacuum but the spins still appear to fragment into two parts: a gauge, or dipolar sector [11, 12] contributing closed internal loops of magnetic flux, and a harmonic sector [14] providing the (unsaturated) ferromagnetic moment. This is illustrated Fig. 1d in the context of the dumbbell model of spin ice [10] in which the magnetic moments at the pyrochlore lattice sites are mapped to flux carrying needles [11]. The four holmium moments, when replaced by needles joining tetrahedron centre I to neighbouring centres J can be decomposed in this spirit. Taking the first element to represent the apical spin:

$$\begin{aligned}
 [M_{IJ}] &= [1, 1, -1, -1] \\
 &= \left[1, -\frac{1}{3}, -\frac{1}{3}, -\frac{1}{3}\right] + \left[0, \frac{4}{3}, -\frac{2}{3}, -\frac{2}{3}\right] \quad (1) \\
 &= [M_{IJ}]_h + [M_{IJ}]_d
 \end{aligned}$$

Each flux runs in a particular direction such that $M_{IJ} = -M_{JI}$ with the convention that an element entering a tetrahedron has a negative sign. The configurations are divergence free. The dipolar fragments, $[M_{IJ}]_d$ whose loops give the residual entropy are restricted to the kagome planes [43] and the harmonic fragments, $[M_{IJ}]_h$, identical for each unit cell give the ferromagnetic order.

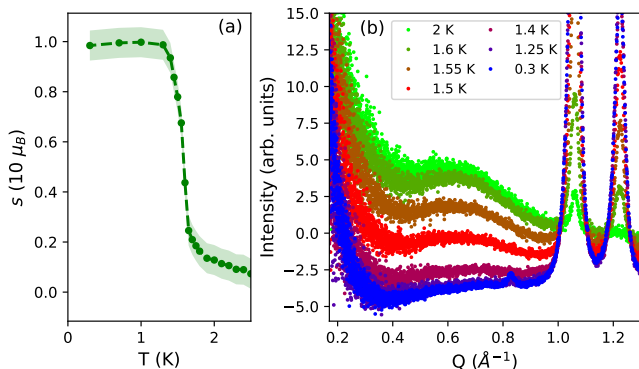


FIG. 5. (a) Refined component s as a function of temperature in the proposed fragmented structure (See text). The shaded region shows the error bars. (b) Zoom in the low Q part of the diffractograms across the Ho transition between 2 and 0.3 K measured on WISH@ISIS, after subtraction of the 100 K data. A negative intensity is observed at low temperature because of the paramagnetic scattering present in the high temperature data. The small peak at 0.8 \AA^{-1} at 0.3 K is due to the ordering of the Ho_2O_3 impurity.

This state is a combination of three partially ordered Γ_9 states aligned along orthogonal [100] cubic axes [14]. As a consequence, $[M_{IJ}]_h$ can be written as the sum of three cubic $[M_{IJ}]$ field sets of amplitude $\frac{1}{3}$. The magnetic Bragg peaks associated with the proposed state are thus identical in a powder sample to those of a (Γ_9) spin ice state and these two possibilities cannot be distinguished directly in our experiments. However, specific modelling of the ordered moment can give an indication of the true nature of the ground state. We have refined our diffractograms considering a thermal spin length s in the harmonic term $[M_{IJ}]_h$:

$$[M_{IJ}]_h = \left[s, -\frac{s}{3}, -\frac{s}{3}, -\frac{s}{3} \right]. \quad (2)$$

The ordered moment is then $s \times m_{\text{Ho}} \approx s \times 10 \mu_{\text{B}}$. As shown in Fig. 5a, we observe a sharp rise in s through the transition, to a saturated moment close to $s = 1$. This result, combined with the residual entropy and the perpetual dynamics down to the lowest temperature are all consistent with the existence of the fragmented ferromagnetic state.

A mechanism for the transition to this special ordered state is however not trivial. The Ru^{4+} ions in the Γ_5 structure create fields at the Ho^{3+} sites lying in the local (x, y) planes, perpendicular to holmium moment. As Ho^{3+} is a non-Kramers ion it is blind to these fields. As a consequence there are no possible bilinear couplings between the two sets of moments, and therefore no molecular fields analogous to those of the iridates [20–22, 46], without relaxation of the ruthenium moments out of their local easy planes.

Our preliminary Monte Carlo results, including a nearest neighbor spin ice term between Ho moments, an easy-plane term favouring the Γ_5 state for the Ru sublattice

and a coupling between Ho and Ru sublattices, show that as Ho-Ho spin ice correlations grow, a tilt of the Ru moments is induced generating an effective ferromagnetic coupling between Ho^{3+} ions. However, in this simple approach the obtained ground state is always a fully ordered Γ_9 state. The selection of the fragmented ferromagnetic state would need an additional term which pushes the magnetisation away from the [100] axes towards the body diagonals. At the molecular field level, this corresponds to a repulsive self-consistent field with cubic symmetry whose action is shown in detail in the supplementary material [36]. Such a term could originate in the interaction between the magnetic and electronic degrees of freedom on the Ru sublattice as proposed for iridate compounds [47, 48].

This mechanism is clearly a fragile compromise which could be influenced by other perturbations, particularly impurities and boundaries between ordered domains. In the absence of magnetic monopoles and with the imposition of topological constraints, boundaries play a very influential role [49–51]. The frustration they cause could, in itself be enough to explain the unsaturated moment with “arctic-circle” freezing effects running deep into the bulk sample [52, 53]. Whether the unsaturated moment is due to such bulk versus surface effects or to the specific mechanisms we have proposed, impurities could also have a profound effect. Indeed, we have observed a small increase in the average low temperature Ho ordered moment ($7.2 \mu_{\text{B}}$) in an aged sample, for which an impurity phase of RuO_2 had grown. This change hints at a configurational order-by-disorder effect [54, 55] in which the configurational disorder drives the system towards a more ordered ground state.

A key feature of the proposed fragmented phase is that the dipolar fragment is expected to give rise to a diffuse scattering signal [11], characteristic of the dipolar correlations associated with the emergent field, as previously observed in the kagome ice phase of spin ice [43, 56]. Above the holmium transition a broad bump between $0.4\text{--}0.8 \text{ \AA}^{-1}$ in the diffuse scattering is observed, compatible with magnetic scattering from a powder of spin ice [57] (See Fig. 5b). Below the transition there is a fall in scattering intensity, with a shift of the intensity to small wave vector, which does not resemble the kagome ice scattering. This could signal the build up of some ferromagnetic correlations in the kagome planes within the proposed state. Analogous behaviour is seen for experiments on $\text{Ho}_2\text{Ti}_2\text{O}_7$ and for model systems with an applied field tilted away from the [111] axis [58].

The extremely sharp specific heat peak, domains of modest size, rounded step function for the ordered moment and changing dynamics through the transition are reminiscent of a rounded first order transition in which the domains fluctuate between competing ordered states over a narrow temperature range. With the development of bigger domains, one would expect the fluctuations to become non-ergodic, the specific heat to extrapolate to a cusp and the entropy to show a discontinuity, correspond-

ing to the latent heat of the transition. The rapid fall in entropy of $\Delta S \approx \frac{1}{4} \ln(2)$ through the transition could be a vestige of such a discontinuity. The transition could still be second order but with an extremely narrow critical region. It is clearly correlated with monopole expulsion, so that the resulting topological constraints could lead to an unconventional topological transition as in the case of model spin ice under pressure [59]. In high magnetic fields, we might expect further ordering out of the fragmented ferromagnetic phase into the ordered monopole crystal phase [20, 21, 43, 60, 61]. Indeed a small anomaly is observed in our data for M vs H at around 1.7 T [36] which is on the correct scale to be a signature of this.

In conclusion, we have shown that in $\text{Ho}_2\text{Ru}_2\text{O}_7$ the Ru^{4+} ions order in the Γ_5 easy plane antiferromagnetic state, which does not couple directly to the holmium moments and does not yield a direct mechanism for their partial ordering into ferromagnetic structure at 1.55 K. The Ho partially ordered moment, the residual entropy and the dynamics from ac susceptibility measurements are compatible with a specific fragmented ferromagnetic state with the resultant moment lying along the [111] direction of the pyrochlore lattice and we offer a phenomenological ordering mechanism that could drive such

a state. Nevertheless, in the absence of a kagome ice like diffuse scattering down to base temperature, we cannot entirely rule out a more generic unsaturated state with ordering along a [100] axis, frustrated by domain boundaries and non-ergodicity; although the ensemble of observables would then be a remarkable coincidence. We hope that the present work will motivate future projects aimed at the Ho ordering. In particular, the recent synthesis of single crystals [62] is promising, while understanding the ordering mechanism requires insight beyond lowest order perturbation theory.

ACKNOWLEDGMENTS

We thank Michel Gingras, Jean-Marie Stéphan and Slava Rychkov for useful discussions. We thank Pierre Lachkar for technical support on the PPMS and for the synthesis. We thank Carley Paulsen for the use of his magnetometers. We acknowledge financial support from the ‘‘Agence Nationale de la Recherche’’ under Grant No. ANR-19-CE30-0040. PCWH also thanks the IHES for hospitality.

-
- [1] J. S. Gardner, M. J. P. Gingras, and J. E. Greedan, Magnetic pyrochlore oxides, *Reviews of Modern Physics* **82**, 53 (2010).
- [2] M. J. Harris, S. T. Bramwell, D. F. McMorrow, T. Zeiske, and K. W. Godfrey, Geometrical frustration in the ferromagnetic pyrochlore $\text{Ho}_2\text{Ti}_2\text{O}_7$, *Physical Review Letters* **79**, 2554 (1997).
- [3] S. T. Bramwell and M. J. Gingras, Spin ice state in frustrated magnetic pyrochlore materials, *Science* **294**, 1495 (2001).
- [4] B. C. den Hertog and M. J. P. Gingras, Dipolar interactions and origin of spin ice in Ising pyrochlore magnets, *Physical Review Letters* **84**, 3430 (2000).
- [5] A. P. Ramirez, A. Hayashi, R. J. Cava, R. Siddharthan, and B. S. Shastry, Zero-point entropy in ‘spin ice’, *Nature* **399**, 333 (1999).
- [6] S. R. Giblin, M. Twengström, L. Bovo, M. Ruminy, M. Bartkowiak, P. Manuel, J. C. Andresen, D. Prabhakaran, G. Balakrishnan, E. Pomjakushina, C. Paulsen, E. Lhotel, L. Keller, M. Frontzek, S. C. Capelli, O. Zaharko, P. A. McClarty, S. T. Bramwell, P. Henelius, and T. Fennell, Pauling entropy, metastability, and equilibrium in $\text{Dy}_2\text{Ti}_2\text{O}_7$ spin ice, *Physical Review Letters* **121**, 067202 (2018).
- [7] S. V. Isakov, K. Gregor, R. Moessner, and S. L. Sondhi, Dipolar Spin Correlations in Classical Pyrochlore Magnets, *Physical Review Letters* **93**, 167204 (2004).
- [8] C. L. Henley, Power-law spin correlations in pyrochlore antiferromagnets, *Physical Review B* **71**, 014424 (2005).
- [9] I. A. Ryzhkin, Magnetic relaxation in rare-earth oxide pyrochlores, *Journal of Experimental and Theoretical Physics* **101**, 481 (2005).
- [10] C. Castelnovo, R. Moessner, and S. L. Sondhi, Magnetic monopoles in spin ice, *Nature* **451**, 42 (2008).
- [11] M. E. Brooks-Bartlett, S. T. Banks, L. D. C. Jaubert, A. Harman-Clarke, and P. C. W. Holdsworth, Magnetic-moment fragmentation and monopole crystallization, *Physical Review X* **4**, 011007 (2014).
- [12] E. Lhotel, L. D. C. Jaubert, and P. C. W. Holdsworth, Fragmentation in frustrated magnets: A review, *Journal of Low Temperature Physics* **201**, 710 (2020).
- [13] S. T. Bramwell, Harmonic phase in polar liquids and spin ice, *Nature Communications* **8**, 2088 (2017).
- [14] F. Museum, E. Lhotel, and P. C. W. Holdsworth, Neutron scattering from fragmented frustrated magnets, *Physical Review B* **107**, 214425 (2023).
- [15] A. S. Wills, M. E. Zhitomirsky, B. Canals, J. P. Sanchez, P. Bonville, P. D. de Réotier, and A. Yaouanc, Magnetic ordering in $\text{Gd}_2\text{Sn}_2\text{O}_7$: the archetypal heisenberg pyrochlore antiferromagnet, *Journal of Physics: Condensed Matter* **18**, L37 (2006).
- [16] A. Poole, A. S. Wills, and E. Lelièvre-Berna, Magnetic ordering in the XY pyrochlore antiferromagnet $\text{Er}_2\text{Ti}_2\text{O}_7$: a spherical neutron polarimetry study, *J. Phys.: Condens. Matter* **19**, 452201 (2007).
- [17] S. Petit, E. Lhotel, F. Damay, P. Boutrouille, A. Forget, and D. Colson, Long range order in the dipolar XY antiferromagnet $\text{Er}_2\text{Sn}_2\text{O}_7$, *Physical Review Letters* **119**, 187202 (2017).
- [18] K. Matsuhira, M. Wakeshima, Y. Hinatsu, and S. Takagi, Metal-insulator transitions in pyrochlore oxides $\text{Ln}_2\text{Ir}_2\text{O}_7$, *J. Phys. Soc. Jap.* **80**, 094701 (2011).
- [19] M. Ito, Y. Y. znd M. Kanada, H. Harashina, S. Yoshii, K. Murata, M. Sato, H. Okumura, and K. Kakurai, Nature of spin freezing transition of geometrically frustrated pyrochlore system $R_2\text{Ru}_2\text{O}_7$ (R = rare earth elements

- and Y), *Journal of Physics and Chemistry of Solids* **62**, 337 (2001).
- [20] E. Lefrançois, V. Cathelin, E. Lhotel, J. Robert, P. Lejay, C. V. Colin, B. Canals, F. Damay, J. Ollivier, B. Fåk, L. C. Chapon, R. Ballou, and V. Simonet, Fragmentation in spin ice from magnetic charge injection, *Nature Communications* **8**, 209 (2017).
- [21] V. Cathelin, E. Lefrançois, J. Robert, P. C. Gurucaga, C. Paulsen, D. Prabhakaran, P. Lejay, F. Damay, J. Ollivier, B. Fåk, L. C. Chapon, R. Ballou, V. Simonet, P. C. W. Holdsworth, and E. Lhotel, Fragmented monopole crystal, dimer entropy, and coulomb interactions in $\text{Dy}_2\text{Ir}_2\text{O}_7$, *Physical Review Research* **2**, 032073(R) (2020).
- [22] M. J. Pearce, K. Götze, A. Szabó, T. S. Sikkenk, M. R. Lees, A. T. Boothroyd, D. Prabhakaran, C. Castelnovo, and P. A. Goddard, Magnetic monopole density and antiferromagnetic domain control in spin-ice iridates, *Nature Communications* **13**, 444 (2022).
- [23] D. A. Huse, W. Krauth, R. Moessner, and S. L. Sondhi, Coulomb and liquid dimer models in three dimensions, *Physical Review Letters* **91**, 167004 (2003).
- [24] V. Raban, C. T. Suen, L. Berthier, and P. C. W. Holdsworth, Multiple symmetry sustaining phase transitions in spin ice, *Phys. Rev. B* **99**, 224425 (2019).
- [25] C. Bansal, H. Kawanaka, H. Bando, and Y. Nishihara, Structure and magnetic properties of the pyrochlore $\text{Ho}_2\text{Ru}_2\text{O}_7$: A possible dipolar spin ice system, *Physical Review B* **66**, 052406 (2002).
- [26] M. Rams, A. Zarzycki, A. Pikul, and K. Tomala, Magnetic order and crystal field in $\text{Dy}_2\text{Ru}_2\text{O}_7$ and $\text{Yb}_2\text{Ru}_2\text{O}_7$, *Journal of Magnetism and Magnetic Materials* **323**, 1490 (2011).
- [27] J. S. Gardner, A. L. Cornelius, L. J. Chang, M. Prager, T. Brückel, and G. Ehlers, Spin dynamics in $\text{Ho}_2\text{Ru}_2\text{O}_7$, *Journal of Physics: Condensed Matter* **17**, 7089 (2005).
- [28] C. R. Wiebe, J. S. Gardner, S. J. Kim, G. M. Luke, A. S. Wills, B. D. Gaulin, J. E. Greedan, I. Swainson, Y. Qiu, and C. Jones, Magnetic ordering in the spin-ice candidate $\text{Ho}_2\text{Ru}_2\text{O}_7$, *Physical Review Letters* **93**, 076403 (2004).
- [29] M. W. Gaultois, P. T. Barton, C. S. Birkel, L. M. Misch, E. E. Rodriguez, G. D. Stucky, and R. Seshadri, Structural disorder, magnetism, and electrical and thermoelectric properties of pyrochlore $\text{Nd}_2\text{Ru}_2\text{O}_7$, *J. Phys.: Condens. Matter* **25**, 186004 (2013).
- [30] C. Paulsen, DC magnetic measurements, in *Introduction to Physical Techniques in Molecular Magnetism: Structural and Macroscopic Techniques*, edited by F. Palacio, E. Ressouche, and J. Schweizer (Servicio de Publicaciones de la Universidad de Zaragoza, 2001).
- [31] E. Lhotel, C. V. Colin, and V. Simonet, Nature of the magnetic ground state of $\text{Ho}_2\text{Ru}_2\text{O}_7$ at low temperature., Institut Laue-Langevin (ILL). doi: [10.5291/ILL-DATA.CRG-2975](https://doi.org/10.5291/ILL-DATA.CRG-2975) (2023).
- [32] E. Lhotel, F. Museur, and V. Simonet, Magnetic structure of $\text{Ho}_2\text{Ru}_2\text{O}_7$ at low temperature, STFC ISIS Neutron and Muon Source. doi: [10.5286/ISIS.E.RB2220581-1](https://doi.org/10.5286/ISIS.E.RB2220581-1) (2022).
- [33] L. C. Chapon, P. Manuel, P. Radaelli, C. Benson, L. Perrott, S. Ansell, N. J. Rhodes, D. Raspino, D. Duxbury, E. Spill, and J. Norris, Wish: The new powder and single crystal magnetic diffractometer on the second target station, *Neutron News* **22**, 22 (2011), <https://doi.org/10.1080/10448632.2011.569650>.
- [34] F. Museur, E. Lhotel, and V. Simonet, Low energy magnetic excitations of $\text{Ho}_2\text{Ru}_2\text{O}_7$, STFC ISIS Neutron and Muon Source. doi: [10.5286/ISIS.E.RB2190160-1](https://doi.org/10.5286/ISIS.E.RB2190160-1) (2022).
- [35] E. Lhotel, F. Museur, and V. Simonet, Low energy magnetic excitations of Ho_2O_3 , STFC ISIS Neutron and Muon Source. doi: [10.5286/ISIS.E.RB2390129-1](https://doi.org/10.5286/ISIS.E.RB2390129-1) (2023).
- [36] Supplementary material, which includes details on structural properties, the “high” temperature characterization, “low” temperature magnetic properties, the specific heat and ac susceptibility data analysis, inelastic neutron scattering measurements and a discussion about ferromagnetism along [111] with a repulsive cubic field.
- [37] J. Rodríguez-Carvajal, Recent advances in magnetic structure determination by neutron powder diffraction, *Physica B* **192**, 55 (1993).
- [38] N. Taira, M. Wakeshima, Y. Hinatsu, A. Tobo, and K. Ohoyama, Magnetic structure of pyrochlore-type $\text{Er}_2\text{Ru}_2\text{O}_7$, *Journal of Solid State Chemistry* **176**, 165 (2003).
- [39] Y. Wang, T. Reeder, Y. Karaki, J. Kindervater, T. Halloran, N. Maliszewskyj, Y. Qiu, J. A. Rodriguez, S. Gladchenko, S. M. Koohpayeh, S. Nakatsuji, and C. Broholm, Monopolar and dipolar relaxation in spin ice $\text{Ho}_2\text{Ti}_2\text{O}_7$, *Science Advances* **7**, eabg0908 (2021).
- [40] F. Morineau, V. Cathelin, P. C. W. Holdsworth, S. R. Giblin, G. Balakrishnan, K. Matsuhira, C. Paulsen, and E. Lhotel, Satisfaction and violation of the fluctuation-dissipation relation in spin ice materials, arXiv:2410.12548 (2024).
- [41] L. D. C. Jaubert and P. C. W. Holdsworth, Magnetic monopole dynamics in spin ice, *Journal of Physics: Condensed Matter* **23**, 164222 (2011).
- [42] K. Matsuhira, Z. Hiroi, T. Tayama, S. Takagi, and T. Sakakibara, A new macroscopically degenerate ground state in the spin ice compound $\text{Dy}_2\text{Ti}_2\text{O}_7$ under a magnetic field, *Journal of Physics: Condensed Matter* **14**, L559 (2002).
- [43] R. Moessner and S. L. Sondhi, Theory of the [111] magnetization plateau in spin ice, *Physical Review B* **68**, 064411 (2003).
- [44] G. Möller and R. Moessner, Magnetic multipole analysis of kagome and artificial spin-ice dipolar arrays, *Physical Review B* **80**, 140409(R) (2009).
- [45] G.-W. Chern, P. Mellado, and O. Tchernyshyov, Two-stage ordering of spins in dipolar spin ice on the kagome lattice, *Physical Review Letters* **106**, 207202 (2011).
- [46] E. Lefrançois, L. Mangin-Thro, E. Lhotel, J. Robert, S. Petit, V. Cathelin, H. E. Fischer, C. V. Colin, F. Damay, J. Ollivier, P. Lejay, L. C. Chapon, V. Simonet, and R. Ballou, Spin decoupling under a staggered field in the $\text{Gd}_2\text{Ir}_2\text{O}_7$ pyrochlore, *Physical Review B* **99**, 060401(R) (2019).
- [47] P. Goswami, B. Roy, and S. Das Sarma, Competing orders and topology in the global phase diagram of pyrochlore iridates, *Physical Review B* **95**, 085120 (2017).
- [48] K. Ladovrechis, T. Meng, and B. Roy, Competing magnetic orders and multipolar Weyl fermions in 227 pyrochlore iridates, *Physical Review B* **103**, L241116 (2021).
- [49] L. Bovo, X. Moya, D. Prabhakaran, Y.-A. Soh, A. T. Boothroyd, N. D. Mathur, G. Aeppli, and S. T. Bramwell, Restoration of the third law in spin ice thin films, *Nature Communications* **5**, 3439 (2014).
- [50] L. D. C. Jaubert, T. Lin, T. S. Opel, P. C. W.

- Holdsworth, and M. J. P. Gingras, Spin ice thin film: Surface ordering, emergent square ice, and strain effects, *Physical Review Letters* **118**, 207206 (2017).
- [51] E. Lantagne-Hurtubise, J. G. Rau, and M. J. P. Gingras, Spin-ice thin films: Large- n theory and monte carlo simulations, *Physical Review X* **8**, 021053 (2018).
- [52] N. Allegra, J. Dubail, J.-M. Stéphan, and J. Viti, Inhomogeneous field theory inside the arctic circle, *Journal of Statistical Mechanics: Theory and Experiment* **2016**, 053108 (2016).
- [53] A. D. King, J. Coraux, B. Canals, and N. Rougemaille, Magnetic arctic circle in a square ice qubit lattice, *Physical Review Letters* **131**, 166701 (2023).
- [54] J. Villain, R. Bidaux, J.-P. Carton, and R. Conte, Order as an effect of disorder, *Journal de Physique France* **41**, 1263 (1980).
- [55] V. S. Maryasin and M. E. Zhitomirsky, Order from structural disorder in the xy pyrochlore antiferromagnet $\text{Er}_2\text{Ti}_2\text{O}_7$, *Physical Review B* **90**, 094412 (2014).
- [56] Y. Tabata, H. Kadowaki, K. Matsuhira, Z. Hiroi, N. Aso, E. Ressouche, and B. Fåk, Kagomé ice state in the dipolar spin ice $\text{Dy}_2\text{Ti}_2\text{O}_7$, *Physical Review Letters* **97**, 257205 (2006).
- [57] A. M. Hallas, J. A. M. Paddison, H. J. Silverstein, A. L. Goodwin, J. R. Stewart, A. R. Wildes, J. G. Cheng, J. S. Zhou, J. B. Goodenough, E. S. Choi, G. Ehlers, J. S. Gardner, C. R. Wiebe, and H. D. Zhou, Statics and dynamics of the highly correlated spin ice $\text{Ho}_2\text{Ge}_2\text{O}_7$, *Physical Review B* **86**, 134431 (2012).
- [58] A. A. Turrini, A. Harman-Clarke, G. Haeseler, T. Fennell, I. G. Wood, P. Henelius, S. T. Bramwell, and P. C. W. Holdsworth, Tunable critical correlations in kagome ice, *Physical Review B* **105**, 094403 (2022).
- [59] L. D. C. Jaubert, J. T. Chalker, P. C. W. Holdsworth, and R. Moessner, Spin ice under pressure: Symmetry enhancement and infinite order multicriticality, *Physical Review Letters* **105**, 087201 (2010).
- [60] T. Sakakibara, T. Tayama, Z. Hiroi, K. Matsuhira, and S. Takagi, Observation of a liquid-gas-type transition in the pyrochlore spin ice compound $\text{Dy}_2\text{Ti}_2\text{O}_7$ in a magnetic field, *Phys. Rev. Lett.* **90**, 207205 (2003).
- [61] O. A. Petrenko, M. R. Lees, and G. Balakrishnan, Magnetization process in the spin-ice compound $\text{Ho}_2\text{Ti}_2\text{O}_7$, *Phys. Rev. B* **68**, 012406 (2003).
- [62] B. K. Patel, M. T. Kolambage, C. D. McMillen, and J. W. Kolis, Hydrothermal synthesis of lanthanide ruthenate single crystals, *Journal of Crystal Growth* **602**, 126979 (2023).
- [63] D. Staško, F. Hájek, K. Vlášková, J. Kaštil, M. Henrique, and M. Klicpera, Robust pinned magnetisation in $\text{A}_2\text{Ir}_2\text{O}_7$ iridates, the case of $\text{Er}_2\text{Ir}_2\text{O}_7$ and $\text{Lu}_2\text{Ir}_2\text{O}_7$ flux-grown single crystals, *Sci. Rep.* **14**, 21773 (2024).
- [64] W. K. Zhu, M. Wang, B. Seradjeh, F. Yang, and S. X. Zhang, Enhanced weak ferromagnetism and conductivity in hole-doped pyrochlore iridate $\text{Y}_2\text{Ir}_2\text{O}_7$, *Phys. Rev. B* **90**, 054419 (2014).
- [65] E. Lefrançois, V. Simonet, R. Ballou, E. Lhotel, A. Hadj-Azzem, S. Kodjikian, P. Lejay, P. Manuel, D. Khalyavin, and L. C. Chapon, Anisotropy-tuned magnetic order in pyrochlore iridates, *Phys. Rev. Lett.* **114**, 247202 (2015).
- [66] S. T. Bramwell, M. J. Harris, B. C. den Hertog, M. J. P. Gingras, J. S. Gardner, D. F. McMorrow, A. R. Wildes, A. L. Cornelius, J. D. M. Champion, R. G. Melko, and T. Fennell, Spin correlations in $\text{Ho}_2\text{Ti}_2\text{O}_7$: A dipolar spin ice system, *Physical Review Letters* **87**, 047205 (2001).
- [67] O. V. Lounasmaa, Specific heat of holmium metal between 0.38 and 4.2°K, *Physical Review* **128**, 1136 (1962).
- [68] G. Mennenga, L. de Jongh, and W. Huiskamp, Field dependent specific heat study of the dipolar Ising ferromagnet LiHoF_4 , *Journal of Magnetism and Magnetic Materials* **44**, 59 (1984).
- [69] S. Rosenkranz, A. P. Ramirez, A. Hayashi, R. J. Cava, R. Siddharthan, and B. S. Shastry, Crystal-field interaction in the pyrochlore magnet $\text{Ho}_2\text{Ti}_2\text{O}_7$, *J. Appl. Phys.* **87**, 5914 (2000).
- [70] P. Henelius, T. Lin, M. Enjalran, Z. Hao, J. G. Rau, J. Altosaar, F. Flicker, T. Yavorskii, and M. J. P. Gingras, Frustration and competing orders in the prototypical $\text{Dy}_2\text{Ti}_2\text{O}_7$ spin ice material, *Physical Review B* **93**, 024402 (2016).

Ferromagnetic fragmented ground state in the pyrochlore $\text{Ho}_2\text{Ru}_2\text{O}_7$: Supplemental Material

S-I. STRUCTURAL PROPERTIES AND DIFFRACTION DATA REFINEMENT

X-ray measurements at ambient temperature show that the $\text{Ho}_2\text{Ru}_2\text{O}_7$ crystallizes as expected in the $\text{Fd}\bar{3}\text{m}$ pyrochlore structure, with a lattice parameter $a = 10.14 \text{ \AA}$. An impurity phase of Ho_2O_3 ($\text{Ia}\bar{3}$, $a = 10.60 \text{ \AA}$) was detected in our sample, representing an amount of 1.58 %.

Neutron diffraction measurements were performed on the diffractometer D1B@ILL, with $\lambda = 2.52 \text{ \AA}$ on a 3 g powder sample. The sample was contained in a vanadium sample holder and cooled down with a ^4He orange cryostat. The diffractogram was first refined at 120 K, above the temperature of the magnetic transitions, using the FULLPROF software and the expected $\text{Fd}\bar{3}\text{m}$ pyrochlore structure was recovered (See Figure S1). At 10 K, the parameter for the position of the oxygen is $x = 0.335$ and the lattice constant is $a = 10.11 \text{ \AA}$.

Similar parameters were later obtained on the time-of-flight diffractometer WISH@ISIS. A magnetic signal from Ho_2O_3 could be observed below 1.2 K in these measurements (see Figure 5 of the main article).

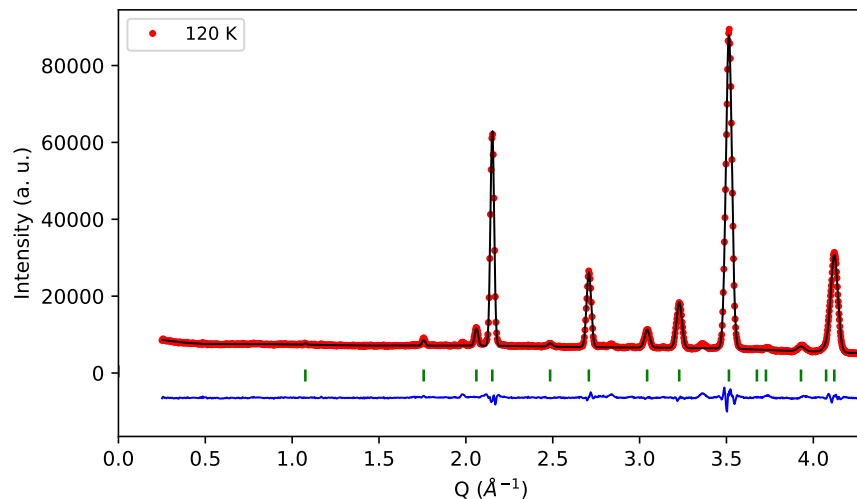


FIG. S1. Diffractogram measured at 120 K on D1B, together with the structural refinement.

As mentioned in the main text, the sample has evolved in time. After the third neutron diffraction scattering experiment on D1B, where the magnetic signal was found to have changed, a check of the sample was performed with X-ray diffraction. We obtained that an impurity of RuO_2 had developed, while the quantity of Ho_2O_3 had grown. The final composition was: (i) $\text{Ho}_2\text{Ru}_2\text{O}_7$: 96.88 % (ii) Ho_2O_3 : 2.10 % (iii) RuO_2 : 1.02 %.

The neutron diffraction data refinement, using the FullProf software, was carried out as follows:

- Above 100 K, the position of the zero angle as well as the scales of the sample phase and sample holder phases were defined.
- Between 10 and 100 K, the Ru magnetic structure was refined together with the lattice parameters. Both ψ_2 and ψ_3 basis states from the Γ_5 representation were tested and yielded the same result. Below about 70 K, the Ru moment stayed constant at $1.2 \mu_B$ per atom.
- Below 10 K, both Ho and Ru magnetic structures were refined in the same phase, as to take into account possible interference effects. A Lorentzian peak width parameter was added to take into account the broadening observed at low temperature. The lattice constant was kept fixed from the values determined at 10 K. The Ho magnetic structure was refined as a harmonic fragment defined in Equation 2 of the main text. To improve the fit, we tried adding various magnetic tilts of allowed symmetries to the Ru magnetic structure, but this didn't show any improvements. It was therefore kept fixed at its 10 K value.

S-II. “HIGH” TEMPERATURE CHARACTERIZATION

On Figure S2 we show magnetic and calorimetric characterization measurements of our $\text{Ho}_2\text{Ru}_2\text{O}_7$ sample above 2 K, performed on PPMS and MPMS setups respectively. The specific heat (left) shows an anomaly at about 95 K which corresponds to the temperature of the ruthenium transition. The magnetization does not show any sign of a ZFC-FC effect around the ruthenium transition at 95 K, contrary to what was seen in Ref. 25 (middle figure). The transition is not visible either in a dM/dT analysis. The signature of the Ru transition is expected to be small in magnetization measurements, due to its small moment compared to Ho. In pyrochlore iridates, the ZFC-FC effect at the Ir transition has been attributed to the uncompensated moments at the boundaries between domains [63] and is possibly reinforced when pinning is present due to defects [64, 65]. The absence of such an effect in our $\text{Ho}_2\text{Ru}_2\text{O}_7$ sample could be the sign of a good quality of the sample.

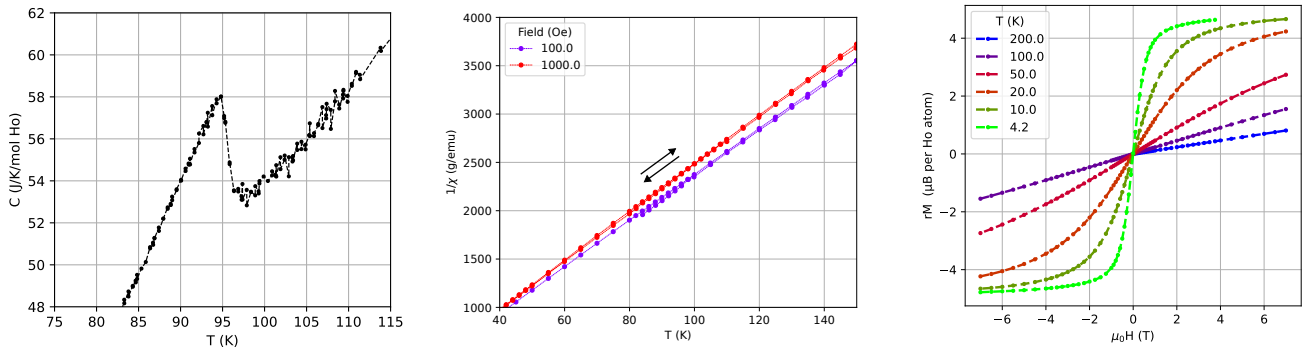


FIG. S2. (left) Specific heat C vs temperature T showing the Ru transition at 95 K. (middle) Zoom in H/M vs T in the Ru transition region for $H = 100$ and 1000 Oe measured with a ZFC-FC protocol. (right) Magnetization M vs field H for several temperatures between 2 and 300 K.

S-III. “LOW” TEMPERATURE MAGNETIC PROPERTIES

At 125 mK and 6 T, the magnetization reaches about $4.75 \mu_B$ per Ho atom (See Figure S3(left)). For a pyrochlore magnet with a strong Ising anisotropy along the local $\langle 111 \rangle$ axes, the powder average saturation magnetization per spin is one half of the magnetic moment μ_{\parallel} [66]. Our measurement is thus consistent with a Ho^{3+} ion with a strong Ising anisotropy. The corresponding Ho magnetic moment μ_{\parallel} would be $9.5 \mu_B$. This value is small compared to the $9.8\text{--}9.9 \mu_B$ value reported in other Ho pyrochlores and obtained from the crystal electric field calculations. This difference may be due to the presence of the impurity phase, whose mass has not been taken into account.

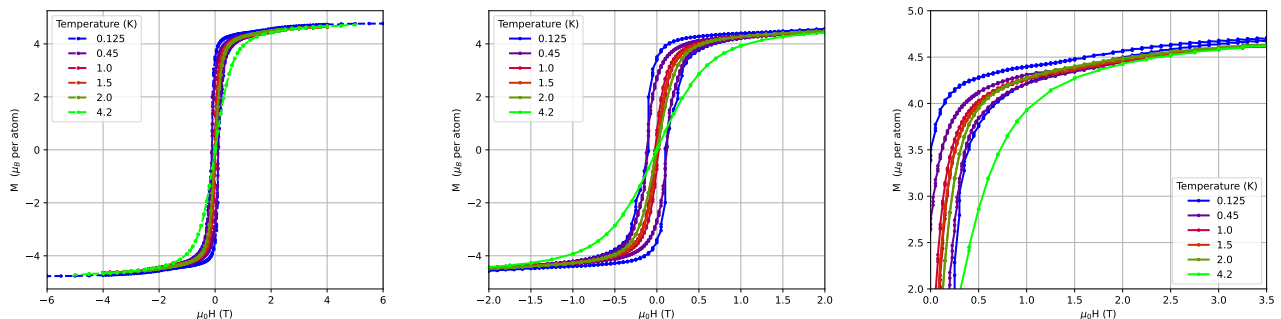


FIG. S3. M vs H at several temperatures between 125 mK and 4.2 K: (left) up to 6 T; (middle) zoom in the hysteresis; (right) zoom in the inflexion point.

An irreversibility is observed at low temperature between the ZFC and FC curves, where the field-cooled behavior suggests a ferromagnetic transition (See Figure S4). Given the scale of the effective ferromagnetic exchange in Ho

pyrochlores ($J_{\text{eff}} \approx 2$ K), it is natural to associate this transition to a magnetic ordering on the Ho sublattice. The amplitude of the ZFC-FC effect is large, indicating the presence of significant energy barriers below the transition. The irreversibility is suppressed when increasing the magnetic field and has disappeared for $H = 3000$ Oe.

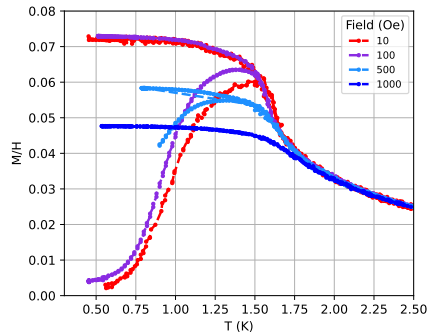


FIG. S4. M/H vs T measured in a ZFC-FC protocol at several fields. The ZFC state was cooled from 4.2 K.

An hysteresis is observed in the M vs H curves below the Ho transition (See Figure S3(middle)). An anomaly is observed around 1.7 T close to the saturation at low temperature (See Figure S3(right)). The interpretation of this effect is hard due to the powder average, but it could be reminiscent from the transition observed between the kagome ice state and the saturated monopole crystal when a field is applied along [111], in spin ices [60, 61] and $\text{Ho}_2\text{Ir}_2\text{O}_7$ [20].

S-IV. SPECIFIC HEAT DATA ANALYSIS

The magnetic specific heat of $\text{Ho}_2\text{Ru}_2\text{O}_7$ is shown in the main article, Figure 3. To obtain this magnetic contribution in the temperature range < 25 K from the total specific heat (see Figure S5), one must subtract the contributions from both the nucleus and the lattice.

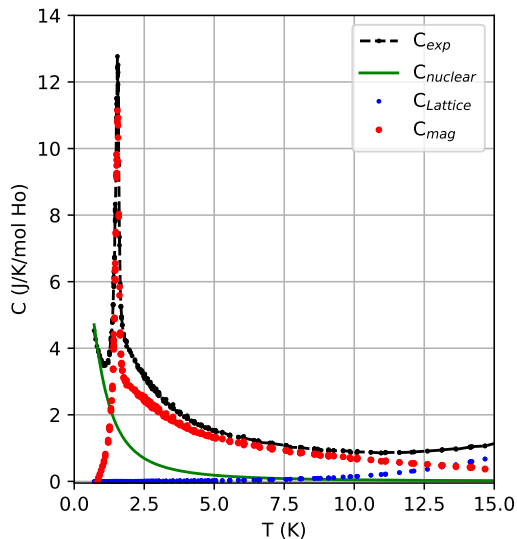


FIG. S5. Measured specific heat in black, nuclear contribution in green, lattice contribution in blue, and subtraction in red

Below 1 K, the rise in specific heat is caused by hyperfine contribution coming from the ^{165}Ho nucleus. Its $I = 7/2$ nuclear spin is split by the interaction with the electronic spin. The corresponding contribution can be obtained from

a $2I + 1 = 8$ level system obeying the following Hamiltonian:

$$\mathcal{H}_N = A_{\parallel} I_z + P \left(I_z^2 - \frac{1}{3} I(I+1) \right) \quad (\text{S1})$$

A_{\parallel} is the strength of the hyperfine interaction, which splits the nuclear levels evenly, and P is the quadrupole interaction, driven by the average quadrupole electronic moment, which modifies the splitting between high and low I_z . The computation of the associated specific heat for one nucleus is straightforward:

$$C_N = \frac{\partial \langle E \rangle}{\partial T} = \frac{\partial}{\partial T} \left(k_B T^2 \frac{\partial \ln Z}{\partial T} \right) = \frac{\sum_{i=-I}^I \sum_{j=-I}^I (E_i^2 - E_i E_j) \exp\left(\frac{-E_i - E_j}{k_B T}\right)}{(k_B T)^2 \sum_{i=-I}^I \sum_{j=-I}^I \exp\left(\frac{-E_i - E_j}{k_B T}\right)} \quad (\text{S2})$$

This expression could in theory be fitted to the data, but we could not accurately collect enough data points at low temperature to obtain a reliable fit. Indeed, below approximately 700 mK, the increase in specific heat and the decrease in grease conductivity cause the sample to become decoupled from the sample holder. This effect is amplified by the fact that we have a powder sample.

For this reason, we chose to manually adjust the rise in specific heat measured below 1 K, comparing our estimates of A_{\parallel} and P with published values measured in other Ho^{3+} systems [66–68]: $A_{\parallel} \in [0.3, 0.4]$, $P \in [0.002, 0.009]$. We find values of $A_{\parallel}/k_B = 0.33$ K, $P/k_B = 0.009$ K work best for our data. This best adjustment is represented in green in Figure S5.

Above 10 K, the lattice degrees of freedom start to contribute significantly. Fitting the data to a Debye model would be difficult because of the ruthenium magnetic transition at $T_N = 95$ K. So as a better approximation we chose to measure the specific heat of the non magnetic analogue $\text{Lu}_2\text{Ru}_2\text{O}_7$: it has the same pyrochlore lattice and therefore a similar phononic structure. However the $\text{Lu}_2\text{Ru}_2\text{O}_7$ measurement needs to be rescaled to account for the different molar mass. The lattice specific heat is a function of the ratio T/Θ_D , where Θ_D is the Debye temperature which varies like the inverse square root of the molar mass. Thus

$$C_{L, \text{HRO}} = C_{L, \text{LRO}} \left(T \times \frac{\Theta_{D, \text{LRO}}}{\Theta_{D, \text{HRO}}} \right) = C_{L, \text{LRO}} \left(T \times \sqrt{\frac{M_{\text{HRO}}}{M_{\text{LRO}}}} \right) \quad (\text{S3})$$

The lattice contribution is shown with blue points in Figure S5.

S-V. AC SUSCEPTIBILITY ANALYSIS

We measured the AC susceptibility using a custom noise susceptometer with a very large bandwidth (1 mHz - 10 kHz). The out of phase susceptibility χ'' shows two bumps, which can be qualitatively associated to two time scales: one dominates below the transition at frequencies below 100 Hz, and another takes over above the transition at frequencies above 1000 Hz.

Therefore, we elected to fit the data using a model with two relaxation times, each contributing a certain fraction of the total signal. We took into account a symmetric spread of relaxation times through a generalized Debye model:

$$\chi(f) = \chi_S + (\chi_T - \chi_S) \left(\frac{\eta}{1 + (2i\pi f \tau_l)^{1-\alpha_l}} + \frac{1-\eta}{1 + (2i\pi f \tau_s)^{1-\alpha_s}} \right) \quad (\text{S4})$$

where χ_T is the DC susceptibility, χ_S is the high frequency limit called adiabatic susceptibility. The two times τ_l and τ_s are the characteristic times for the long (or slow) and short (or fast) processes respectively, with spread parameters α_l and α_s and relative amplitude η . $\alpha = 0$ corresponds to the single time Debye model.

The fits were performed simultaneously on χ' and χ'' . In order to constrain the fit, the times scales were fitted on the χ'' data, then fixed to fit the rest of the parameters on the χ' data. The α parameters were also set to 0 if the amplitude of the related mode is too small. The fits are represented in Figure S6 by dashed lines. They could not be performed accurately below 1 K because the relaxation times become longer than 10^3 seconds.

In Figure S7 we show the parameters of the two modes estimated by the fits. The estimated DC susceptibilities for each mode as well as their sum are shown on the left. The slow mode arises very abruptly at the transition, while the fast mode only gets gradually suppressed below the transition. On the right we show the coefficient α , which characterizes the spread of relaxation times for each mode. It increases for both modes as the temperature is lowered through the transition; however the fast mode seems to have much broader distribution of relaxation times above the transition than the slow mode.

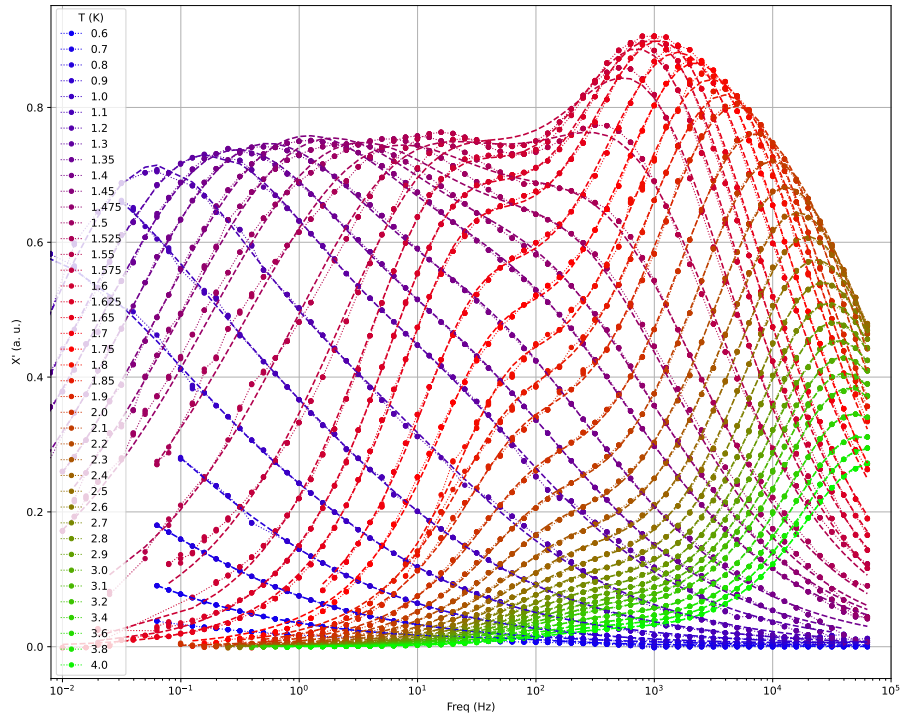
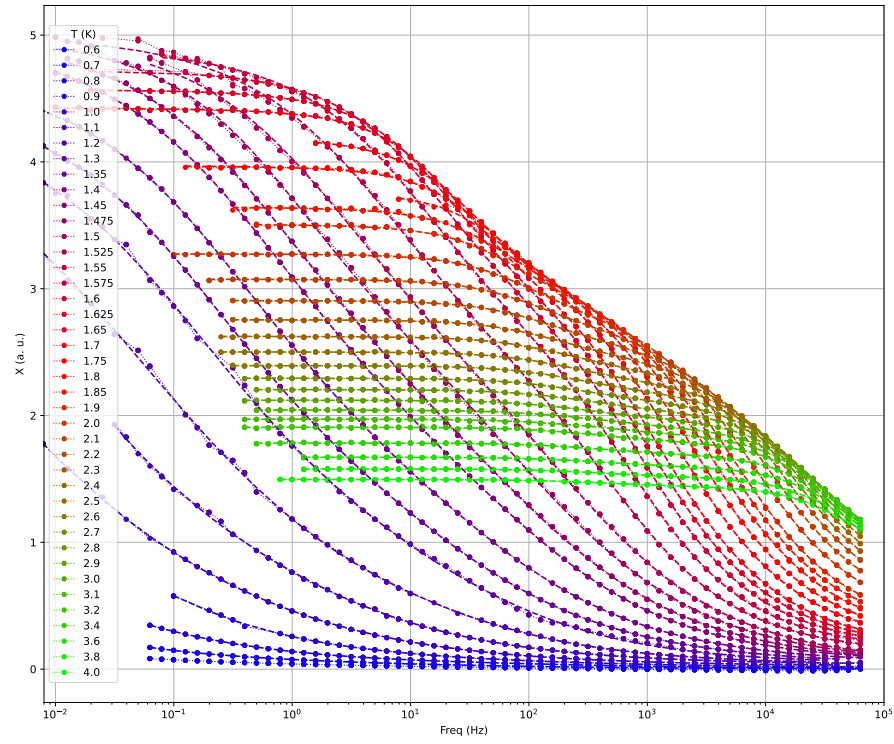


FIG. S6. (Top) In phase χ' and (bottom) and out of phase χ'' susceptibilities measured on the noise magnetometer. The data points are the dots linked by thin dotted lines. The thick dashed line are a fit by the model.

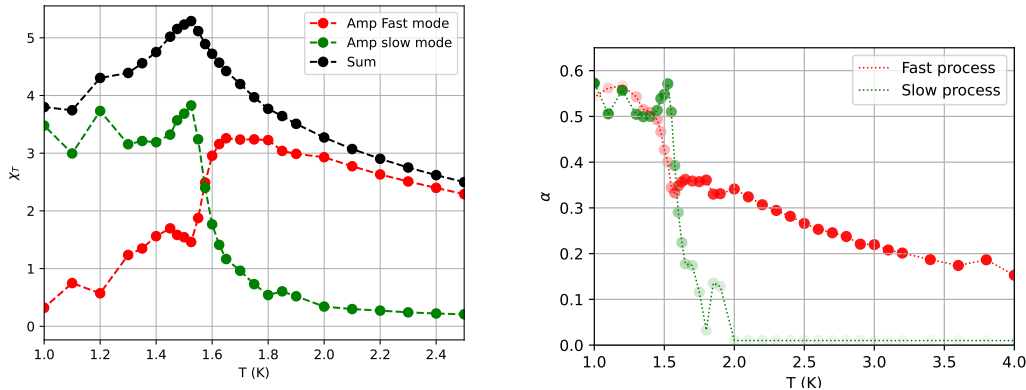


FIG. S7. (left) DC susceptibility of each mode in red and green, and their sum in black. (right) Spread of relaxation times α of each mode. The transparency represents the relative amplitude of the modes.

S-VI. INELASTIC NEUTRON SCATTERING

Two series of experiments were performed at LET@ISIS, in order to detect possible low energy excitations in inelastic neutron scattering measurements. The first set of measurements was performed with four incident energies, $E_i = 2.2, 3.7, 7.52$ and 22.78 meV and at temperatures of 1.5, 20 and 100 K.

At 100 K, these measurements could reveal two non-dispersive excitations centered around positive energy transfers 1.5 and 4.8 meV (See Figure S8(left)). Similar excitations were observed in reference 28. They can be interpreted as transitions between the excited Ho^{3+} crystal electric field states, which are observed between 20 and 28 meV in $\text{Ho}_2\text{Ti}_2\text{O}_7$ [69] and are thus thermally populated at the measured temperature of 100 K. (Note that our higher incident energy - 22.78 meV - was not large enough to observe these levels, but that no signal is observed between 5 and 18 meV, apart from a phonon around 10 meV, whose intensity is stronger at large Q).

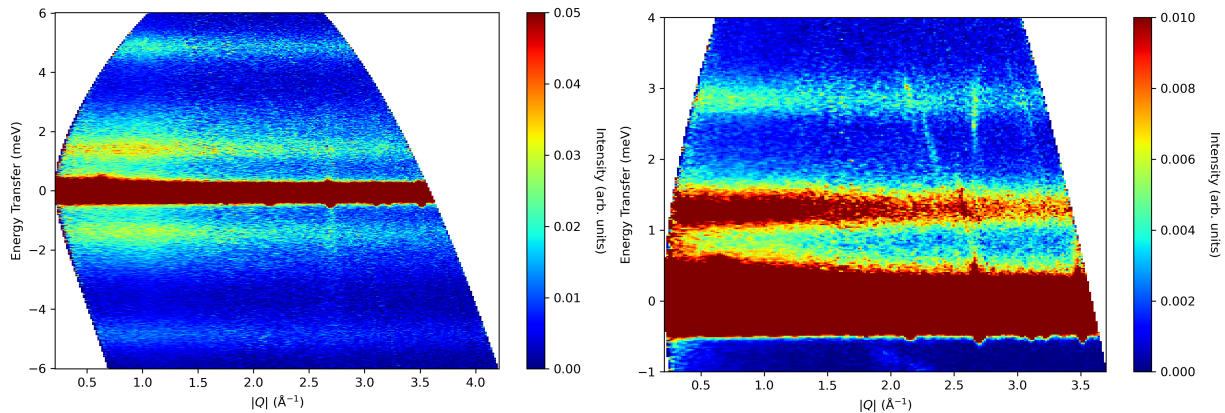


FIG. S8. $S(q, E)$ measured with $E_i = 7.52$ meV at 100 K (left) and 1.5 K (right).

When decreasing the temperature, the signal at negative energy is strongly suppressed and the mode at 4.8 meV disappears (See Figure S9(left)). At 1.5 K, flat modes are nevertheless present at energies of 1.4 and 2.7 meV (See Figures S8(right)). The origin of these well defined excitations is puzzling, given the non-Kramers nature of the Ho^{3+} ion, and the composition of its ground state doublet wave function in pyrochlore oxide series, which is essentially made of $|\pm 8\rangle$ and $|\pm 5\rangle$ components. Indeed transitions between the two states of the doublet cannot be observed in inelastic neutron scattering due to the $\Delta m = 0, \pm 1$ neutron selection rule.

Knowing that an impurity phase of Ho_2O_3 is present in our sample, we have thus measured a powder of Ho_2O_3 in a second set of experiments, at the same temperatures, and with an incoming energy of 7.52 meV. These experiments could confirm that the low energy signal does come from Ho_2O_3 (See Figure S9(right)). Therefore, no clear signal due to $\text{Ho}_2\text{Ru}_2\text{O}_7$ is present at these energies. It would be of interest to probe the system at much lower energies to see if transverse terms can generate an inelastic signal.

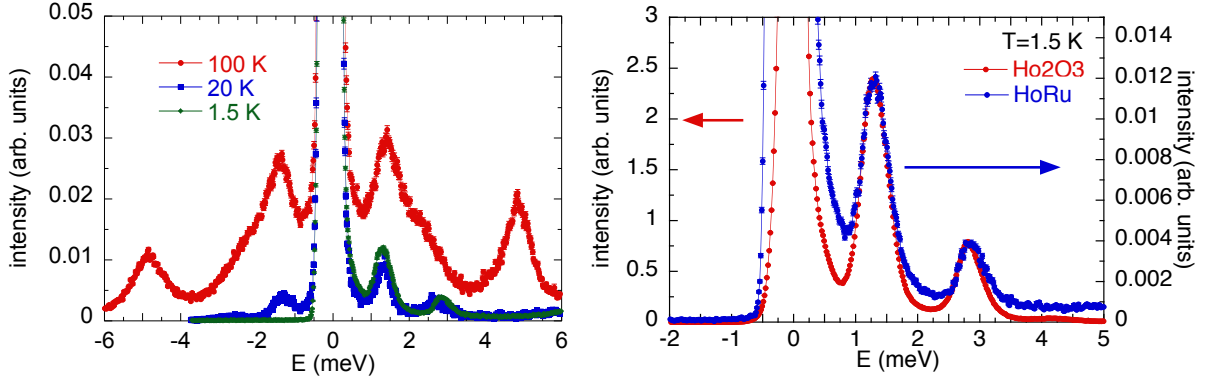


FIG. S9. Neutron intensity vs energy transfer obtained from the integration of $S(Q, E)$ between $Q = 1.05$ and 1.5 \AA^{-1} with $E_i = 7.52 \text{ meV}$. left: for $\text{Ho}_2\text{Ru}_2\text{O}_7$ at 100, 20 and 1.5 K; right: for $\text{Ho}_2\text{Ru}_2\text{O}_7$ and Ho_2O_3 at 1.5 K.

S-VII. FERROMAGNETISM ALONG [111] WITH REPULSIVE CUBIC FIELD

The saturated ferromagnetic state of spin ice is a $q = 0$ state with magnetisation along any one of the [100] directions. Each spin has a projection along the cubic direction of $\frac{1}{\sqrt{3}}$ so that, in the [100] ground state, the vector moment per spin is $\vec{M}^{max} = \frac{1}{\sqrt{3}}\hat{z}$ where \hat{z} is along one of the six possible directions and the moment per spin is taken to be unity.

This should be contrasted with a fragmented ferromagnetic phase with moment along (or against) one of the body centred diagonal directions

$$\begin{aligned} \vec{d}_1 &= \frac{1}{\sqrt{3}}[1, 1, 1], & \vec{d}_2 &= \frac{1}{\sqrt{3}}[1, -1, -1] \\ \vec{d}_3 &= \frac{1}{\sqrt{3}}[-1, -1, 1], & \vec{d}_4 &= \frac{1}{\sqrt{3}}[-1, 1, -1]. \end{aligned} \quad (\text{S5})$$

For \vec{M} lying along one of these axes \hat{d} , the maximum total magnetisation of an up tetrahedron (which we take to be the unit cell of the pyrochlore lattice) is $M_{tet} = 1 + \frac{1}{3} + \frac{1}{3} - \frac{1}{3} = \frac{4}{3}$ so that $\vec{M}^{max} = \frac{1}{4}M_{tet}\hat{d} = \frac{1}{3}\hat{d}$. Making reference to the fragmentation picture we refer to these two states as saturated (the [100] state) and fragmented (the [111] state).

As these two ground states already have cubic symmetry, a self-consistent field term could separate them allowing for the fragmented state to be the preferred low energy state.

The ferromagnetic states would be selected through the generation of a perturbation that lifts the spin ice manifold (quasi)-degeneracy. One possibility is the J_{3a} third neighbour coupling as defined in reference 70. To this we add a quartic term depending on a self-consistent field, $\vec{h}_{eff} = \vec{M}$ whose sign will define which of the ferromagnetic states are selected. A perturbation to the spin ice Hamiltonian could take the form

$$H_1 = -J_{3a} \sum_{ij} \vec{S}_i \cdot \vec{S}_j + \frac{v_0}{4} \sum_{I, N_I} \left(\sum_{j=1,4} \vec{S}_i \cdot \vec{h}_{eff} \right)^2, \quad (\text{S6})$$

where the first sum runs over all third neighbour pairs coupled by J_{3a} [70] and the second runs over all spins separated into N_I unit cells ($N = 4N_I$).

The ground state energies can be estimated for the two states as a function of v_0 .

- In the saturated state, all 3^{rd} neighbour pairs lie parallel to each other, giving an exchange energy of $-12J_{3a}$ per cell, or $-3J_{3a}$ per spin. The self-consistent field is $h_{eff} = \frac{1}{\sqrt{3}}\hat{z}$ so that the perturbation per spin is

$$\epsilon_s = -3J_{3a} + \frac{4v_0}{9}. \quad (\text{S7})$$

- In the fragmented state, the six 3^{rd} neighbour bonds of the apical spins are satisfied, but the 18 others remain frustrated. However, their total contribution will not be zero because of the 2-in-1-out ice rules. This broken

Z_2 symmetry means that the mean of the third neighbour correlation functions for spins in the kagome plane will be $\langle \vec{S}_i \cdot \vec{S}_j \rangle = \frac{1}{9}$ leading to $-4J_{3a}$ per unit cell and $-J_{3a}$ per spin. The self-consistent field is $h_{eff} = \frac{1}{3}\hat{d}$ so that the perturbation energy per spin is $\frac{v_0}{4} \left(\frac{1}{3} + \frac{1}{9}\right)^2 = v_0 \left(\frac{4}{81}\right)$ and the total energy per spin is

$$\epsilon_f = -J_{3a} + \frac{4v_0}{81}. \quad (\text{S8})$$

Putting these two energies equal we find that the fragmented phase becomes stable for

$$v_0 = \frac{81}{16}J_{3a}, \epsilon_f = -\frac{3}{4}J_{3a}. \quad (\text{S9})$$